DEUTSCHES ELEKTRONEN-SYNCHROTRON

DESY 93-160
November 1993

New Results from ZEUS on e-p Collisions at HERA

N. A. Pavel
(ZEUS Collaboration)

II. Institut für Experimentalphysik, Universität Hamburg

ISSN 0418-9833

NOTKESTRASSE 85 - 22603 HAMBURG

To be sure that your preprints are promptly included in the HIGH ENERGY PHYSICS INDEX, send them to (if possible by air mail):

DESY **Bibliothek** **Notkestraße 85** **22603 Hamburg** **Germany**	**DESY-IfH** **Bibliothek** **Platanenallee 6** **15738 Zeuthen** **Germany**

DESY 93-160
November 1993

ISSN 0418-9833

New Results from ZEUS on e-p Collisions at HERA

Nikolaj A. Pavel (ZEUS Collaboration) [1]
II. Institut für Experimentalphysik
Universität Hamburg, FRG

Abstract

At HERA electron proton collisions at very high center of mass (c.m.) energies are produced, opening up a new kinematic range in *e-p* physics. Already in the first year of data-taking many interesting results have been obtained in the field of deep inelastic scattering, photoproduction and new particle search. New results of the ZEUS experiment at HERA, based on the data taken in 1992, are presented and discussed.

Introduction

On May 31, 1992 the first observation of *e-p* collisions in the HERA experiments H1 and ZEUS marked the beginning of the data-taking at the world first electron-proton collider. Since that pioneering run the machine group was able to increase the luminosity greatly reaching $1.8 * 10^{30}\,\mathrm{cm}^{-2}\mathrm{s}^{-1}$ in September '93.

The invariant mass created in the *e-p* collisions at HERA is by one order of magnitude larger than that reached in fixed target experiments. This allows to measure the proton structure function down to x-values of 10^{-4} and to study the photoproduction process at values of the invariant mass W up to 200 GeV. Thus it is possible to investigate physics processes in a completely new kinematic regime.

This report is focussed on results obtained from the analysis of data taken in 1992. After a brief description of the ZEUS detector and running conditions in section 1, results from deep inelastic scattering, photoproduction and the search for new particles will be presented and discussed in section 2-4. Concluding remarks are given in section 5.

1 Data-Taking Conditions

1.1 HERA

At HERA electrons of 26.7 GeV and protons of 820 GeV are brought to collision in the interaction zones of the experiments H1 and ZEUS. HERA is designed to operate with 210 bunches each in the electron and in the proton ring. The design luminosity is $1.5 * 10^{31}\,\mathrm{cm}^{-2}\mathrm{s}^{-1}$.

For the data-taking periods in 1992 nine consecutive bunches were filled for each beam for collisions. In addition two unpaired bunches, one electron and one proton bunch, were circulating for measuring the background event rate from electron-gas and proton-gas interactions.

The electron and proton beam current were typically 1-2 mA and the specific luminosity about $4.\,10^{29}\,\mathrm{cm}^{-2}\mathrm{s}^{-1}\mathrm{mA}^{-2}$. The length of the interaction region, determined by the length of the colliding bunches, was about 20 cm (rms) around the interaction point.

1.2 The ZEUS Detector

ZEUS is a general purpose, magnetic detector with a tracking region surrounded by a high resolution calorimeter as shown in fig. 1.1, followed by a backing calorimeter and a muon detection system. Here only those details which are essential for the understanding of the analysis presented, will be described briefly. A more extensive description can be found in [1, 2].

The principal component used is the high resolution uranium-scintillator calorimeter (CAL) which covers 99.7% of the 4π solid angle. [3]. It is divided into 3 sections: forward (FCAL), barrel (BCAL) and rear (RCAL) calorimeters. The relative thicknesses of the uranium and scintillator layers were chosen to give equal calorimetric response to electrons (or photons) and hadrons. The energy resolution was measured in test beams to be $\sigma_E/E = 0.18/\sqrt{(E)}$ for electrons and $\sigma_E/E = 0.35/\sqrt{(E)}$ for hadrons, where E is measured in GeV.

The scintillator tiles form towers which are segmented longitudinally into electromagnetic (EMC) and hadronic (HAC) cells. Each cell is readout on two sides by PMT's.

The natural radioactivity of the uranium is exploited to set the gain of each PMT to sufficient precision and to monitor very efficiently the overall calibration [3, 4]. The noise distribution, which is dominated by the natural radioactivity, has typically a r.m.s. width of 15 MeV in EMC cells and 25 MeV in HAC cells. The coherent noise between different cells is negligible. However, due to the large number of cells, the noise influences the determination of kinematic quantities in certain region of phase space.

Charged particles are measured by a jet-type drift chamber (CTD) surrounding the beam pipe [5]. It operates in a solenodial magnetic field of 1.43 T. The cylindrical drift chamber layers are organised in nine superlayers [6]. Three of the inner superlayers were read out for this data taking period using a z-by-timing readout system.

Two small ring counters (C5) mounted on the beampipe at the rear of the RCAL give information about the time structure and other properties of the two beams.

[1] invited talk on the International Conference on Hadron Structure, Bratislava,Sept. 1993

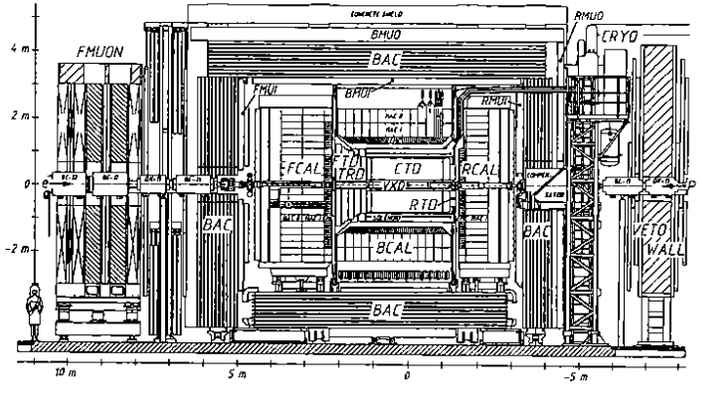

Fig. 1.1. Cross section of the ZEUS detector

The luminosity was determined by the measurement of the rate of hard photons from the Bethe-Heitler bremsstrahlung $ep \rightarrow ep\gamma$ in a lead-scintillator calorimeter placed in the electron beam direction at z=−106 m [7]. A calorimeter installed near to the electron beam at z=−35 m is used to tag photoproduction events by measuring the scattered electron under very small scattering angles.

1.3 Selection of Electron Proton Events

The separation of candidates for e-p collisions from the copious background at early trigger levels is a challenging task. By far the largest background rate is produced by proton-gas interactions.

The calorimeter time information has turned out to be the most powerful handle for rejecting this kind of background events. The time delay for each PMT signal was adjusted such that particles which are emitted from the interaction point (IP) arrive at the calorimeters cells at the time $t = 0$ ns (fig. 1.2). For proton interactions upstream of the detector, energy is deposited in the

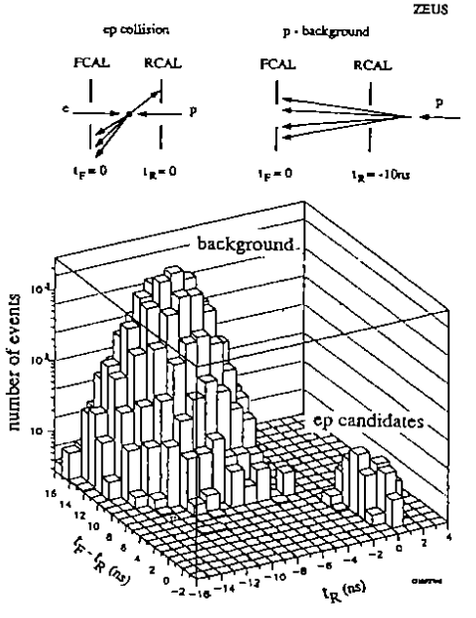

Fig. 1.2. Illustration of beamgas background rejection using the calorimeter time information

rear calorimeter (RCAL) about 12 ns earlier. This time difference corresponds to twice the distance between the IP and the RCAL. As the particles deposit energy in the FCAL at the time $t_F = 0$ ns, the time difference $(t_F - t_R)$ is +12 ns.

The measured distribution of $(t_F - t_R)$ versus t_R is shown in fig. 1.2 for events for which more than 1 GeV was recorded in at least one calorimeter cell both in the FCAL and RCAL. The candidates for e-p collisions can be well separated from the proton beamgas background by suitable cuts in these variables.

The rate of electron-gas and residual proton-gas events was determined using events from the unpaired electron and proton bunches.

Events triggered by cosmic muons or halo muons were removed with the help of topological algorithms in the offline analysis.

Further cuts to reduce the background and to extract a clean event sample depend on the physics process studied and will be reported in the following

sections.

2 Deep Inelastic Scattering

Deep inelastic lepton nucleon scattering (DIS) experiments have played an important role in exploring the hadronic substructure [8, 9] and in developing and testing QCD by inclusive and semi-inclusive processes [10, 11]. Fixed target experiments have been limited to values of $x > 10^{-2}$ for $Q^2 > 4\,\mathrm{GeV}^2/c^2$. HERA allows the extension of measurements to $x \approx 10^{-4}$ at $Q^2 > 10\,\mathrm{GeV}^2/c^2$ and to high W^2, where new phenomena are expected.

2.1 Event Selection and Data Characteristics

The basic deep inelastic e-p scattering process is illustrated in fig. 2.1. The incoming electron couples to a current mediated by γ, Z or $W^{\pm}$, which probes the structure of the proton. Neutral (NC) and charged (CC) current reactions are distinguishable by the signature of a final state electron or by missing transverse momentum.

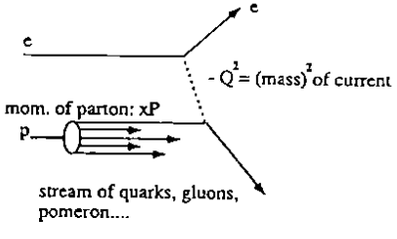

Fig. 2.1. Schematic diagram of deep inelastic e-p scattering

In absence of QED radiation the basic kinematical variables are given by:

$$Q^2 = -q^2 = -(k - k')^2 \tag{2.1}$$

$$x = Q^2/(2Pq) \tag{2.2}$$

$$y = (Pq)/(pk) \tag{2.3}$$

where k and k' are the four-momenta of the initial and final state lepton respectively; P is the initial proton four-momentum. Q^2 is the negative square of the four-momentum transfer and x is the Bjorken scaling variable.

At the Q^2 scale much smaller than m_W^2, the cross section for CC reaction is very small. Nevertheless a couple of spectacular CC events have been observed

in 1992/3 data-taking periods. However, a sizable increase in luminosity is required for a study of CC processes. For the time being the analysis is focussed on NC processes.

For NC events the reconstruction of the kinematic variables can be performed using either energy and angle of the scattered electron or of the hadronic system ot a combination of both. For the analysis presented here, the double angle method (DA) was chosen, because it is less sensitive to scale errors in the energy measurement of the final state [12].

In this method the kinematic variables x_{DA} and Q^2_{DA} are derived from the scattered electron angle ϑ_e and the angle γ_H of a hypothetical massless object balancing the momentum vector of the electron to satisfy four-momentum conservation. The quantity γ_H is determined using the equation:

$$\cos\gamma_H = \frac{(\sum_h p_x)^2 + (\sum_h p_y)^2 - (\sum_h E - p_z)^2}{(\sum_h p_x)^2 + (\sum_h p_y)^2 + (\sum_h E - p_z)^2} \tag{2.4}$$

where the sum $\sum_h$ runs over all calorimeter cells which are not assigned to the scattered electron. p_x, p_y, p_z are the cell energies projected on the axes of the HERA laboratory frame, in which the positive z-axis is the proton direction. The cell angles ϑ are calculated from the geometric center of the cells and the vertex position of the event.

The invariant mass of the hadronic final state W is calculated using the values for x and Q^2 from the DA method:

$$W^2 = Q^2_{DA}\,(\frac{1}{x_{DA}} - 1) + M^2_{prot} \tag{2.5}$$

where M_{prot} is the proton mass. The variable y is determined according to the Jacquet-Blondel method [13]:

$$y_{JB} = \frac{\sum_h (E - p_z)}{2E_e} \tag{2.6}$$

where E_e is the electron beam energy.

The key signature of a NC event is the presence of the scattered electron. Several algorithms, which are based on the information about the transverse and longitudinal shower profile information, were used for an efficient and reliable identification of the scattered electron.

In addition to the event selection criteria discussed in sect. 1.3 the following cuts were applied to obtain a clean sample of DIS events:

- A value of $\delta = \sum(E - p_z) > 35\,\mathrm{GeV}$ was required, where the sum runs over all calorimeter cells. Neglecting effects of particle emission through the rear beampipe hole and initial state QED radiation, NC events have $\delta = 2E_e$. Proton-gas events which have no energy deposited in the RCAL or the C5 counter and therefore pass the before mentioned timing

cuts, have δ close to zero. Also for photoproduction events, where the scattered electron is not seen in the main detector, the quantity δ is significantly smaller than $2E_e$. A cut on δ rejects the major fraction of these backgrounds and reduces the size of the radiative corrections to be applied.

- A fiducial cut around the beampipe hole in RCAL ($|x|, |y| < 16\,\mathrm{cm}$) is imposed to ensure a reliable reconstruction of the impact point of the electron on the face of the RCAL.
- A scattered electron energy of at least 5 GeV, where the efficiency for the electron identification is close to unity, is required.
- A minimum value of y_{JB} of 0.04 is required to retain sufficient energy in the calorimeter to calculate the DA variables.

The event sample left after these cuts is shown in a scatter plot in fig. 2.2. The data populate the Q^2-x-plane down to x values of 10^{-4}, two orders of

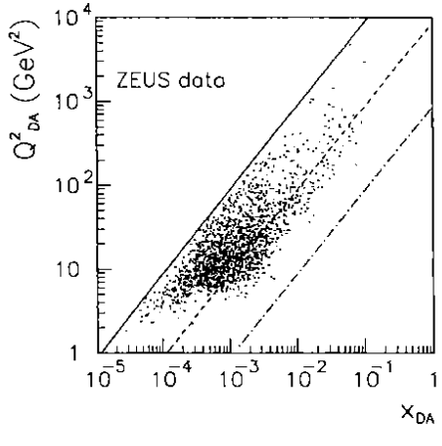

Fig. 2.2. Scatter plot of NC event distribution in the x-Q^2 plane.

magnitude smaller than in previous DIS experiments. Most of the events have a four-momentum transfer in the order of 5 to 100 $\mathrm{GeV}^2/\mathrm{c}^2$, but NC events with a Q^2 up to 2500 $\mathrm{GeV}^2/\mathrm{c}^2$ have been observed. The main interest in the analysis of the first year's data lies in the physics at small x.

2.2 Measurement of F_2

For the Q^2-range studied with the data collected in 1992, the deep inelastic e-p interaction is described by single photon exchange. The double differential cross section is given in terms of the structure functions F_2 and F_L:

$$\frac{d^2\sigma}{dxdQ^2} = \frac{2\pi\alpha^2 Y_+}{xQ^4}\left[F_2(x,Q^2) - \frac{y^2}{Y_+}F_L(x,Q^2)\right](1+\delta_{rad}) \qquad (2.7)$$

where F_L is the longitudinal structure function, $Y_+ = 1 + (1-y)^2$ and δ_{rad} expresses the QED radiative correction term.

From the differential cross section measured in a set of bins in x and Q^2, the structure function F_2 can be extracted. The unfolding of the acceptance and migration of events from the 'true' (x, Q^2) to the reconstructed (x, Q^2) was performed by comparing distributions from the data sample and those from Monte Carlo data, which simulated all effects of the detector and reconstruction inefficiencies. The corrections for QED radiative effects, which are limited in size due to the cut on δ and the use of the DA method, were included in the procedure using the HERACLES program [14].

This gave a bin-by-bin correction factor to the F_2 structure function used as input for the Monte Carlo simulation. The fractional contribution of the F_L term was estimated to be small except for the lowest x and highest y bins, where it reaches $8-10\%$. The total systematic error was determined in each bin by extensive studies and varies between 5 and 20%, see fig. [15]. The main source is the uncertainty in the subtraction of the photoproduction background at high y.

The structure function F_2 is shown as function of x in bins of Q^2 fig. 2.3. The exact values and the systematic errors are tabulated in [16]. The data show a significant rise in F_2 towards low x, increasing by a factor of about 2 when x decreases from 10^{-2} to 10^{-4}.

This result can be interpreted as an increase of the parton density with decreasing x at fixed Q^2, as predicted qualitatively by the BFKL evolution equations [17]. Thus, in the low x region reached at HERA one begins to study objects with a high parton density at Q^2 values where α_s is still small. This will provide an important test of the conventional models of QCD.

The curves overlaid represent the expectation of several extrapolations of parametrizations [18, 19, 20]. The differences are mainly due to the different assumptions made for the x-dependence of the gluon structure function $G(x)$. The dotted line represents the result of a calculation, in which gluons and sea quarks are generated by an dynamical QCD model ([20]).

2.3 Hadronic Energy Flow

The large photon-proton c.m. energies that can be reached HERA, open new possibilities for the study of the hadronic final states in deep inelastic scatter-

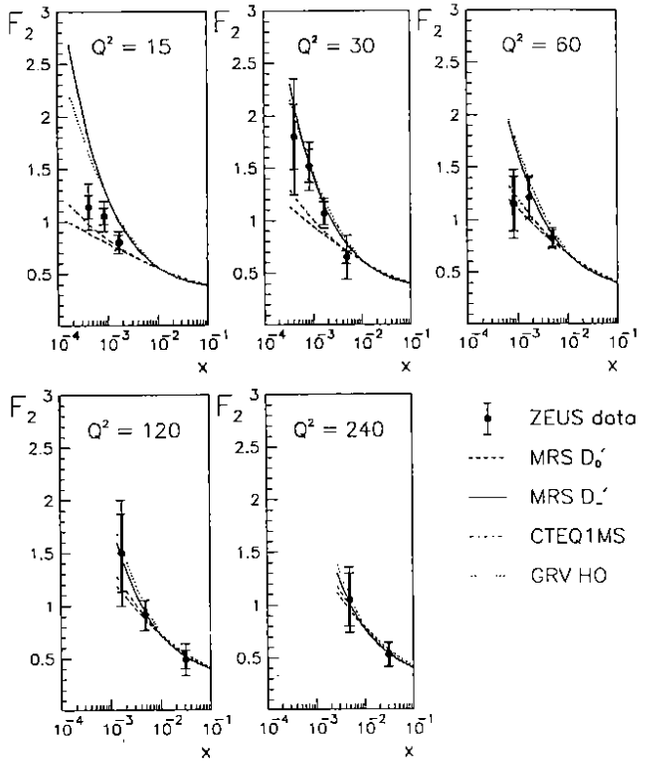

Fig. 2.3. Structure function F_2 versus x for various values of Q^2. The inner and outer error bars represent the statistical error and systematical error added in quadrature, respectively. An overall normalisation error of 7% is not shown. The data are compared with various structure function expectations.

ing. Events with an unambiguous multi-jet structure can be seen directly [21] and make the measurement of jet rates much easier than in the earlier fixed target experiments. First preliminary results on the determination of jet rates from ZEUS data have been presented [22].

A measurement of the hadronic energy flow allows to extend the studies of the hadronic final state to classes of events which cannot be unambiguously classified as n-jet events. This kind of measurement is sensitive to details of the

hard scattering process as well as to soft QCD radiation and hadronization.

The ZEUS detector with its high precision hadron calorimeter is ideally suited for these studies.

In a previous publication uncorrected energy distributions have been compared to various models, which simulate the hadron production in DIS [23]. Many of the models, which give a satisfactory representation of the data at lower energy DIS experiments [24, 25], fail to describe the distributions at HERA energies.

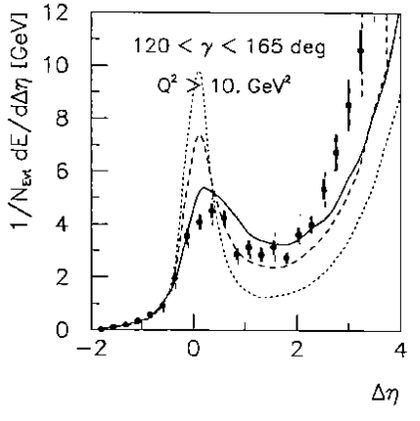

Fig. 2.4. Hadronic energy flow with respect to the direction of γ_H (see text). Model calculations shown are: $O(\alpha_s)$ matrix element + parton shower matched (ME+PS) (full line), $O(\alpha_s)$ matrix element alone (ME) (dashed line), QPM only (dotted line). In all calculation the string fragmentation was used.

For a closer investigation of the QCD processes contributing to the observed energy flow, it is advantageous to study the hadronic energy flow with respect to the angle γ_H (eq.2.4), which in the simple quark parton model (QPM) is the direction of the struck quark. Fig. 2.4 shows the energy flow $dE/d\Delta\eta$, corrected for all effects of detector acceptance and resolution and of QED bremsstrahlung. $\Delta\eta$ is the difference of the pseudorapidity η of the location of energy deposit at the polar angle ϑ and the pseudorapidity which corresponds to the direction defined by the angle γ_H, i.e. $\Delta\eta = \eta - \eta_{\gamma_H}$, where $eta = -\ln(\tan\frac{\vartheta}{2})$ and eta_{γ_H} defined analogously.

The same selection criteria were applied as for the analysis of the inclusive cross section. From these events a subsample was chosen, where the hadron activity associated with the current jet is separated in rapidity space from that associated with the target jet by requiring $\gamma_H > 120°$ [26].

In the QPM the current jet is expected to be centered around $\Delta\eta = 0$, giving rise to a peak in the distribution at this position (dotted line in fig. 2.4). The data show a small but significant shift of the peak position towards the direction of the target jet.

The data are also compared with two other model predictions. One is based on a complete first order α_s matrix element calculation (ME), where only relatively hard QCD processes are considered (dashed line). The other one adds soft QCD radiation modelled by parton showers (full line); the contributions from hard and soft QCD processes are appropiately matched to avoid double counting. [27]. Though none of the models describes all characteristics of the data in a satisfactory manner, one can conclude from the comparison of these two predictions with the data that the shift of the peak is mainly induced by soft QCD processes.

There are two effects which lead to a shift of the peak: first, due to the parton splitting in the parton shower the struck parton acquires an effective mass whereas for the calculation of the angle γ_H one assumes a massless parton. Second, the effective transverse momentum of the parton to which the hard photon couples, is increased due to the spacelike part of the parton shower.

The second important observation is that there is a sizable hadronic activity in the pseudorapidity interval between the current and the target jet. This region is sensitive to the amount of soft gluon radiation and to hadronization effects like the string effect [28].

2.4 Events with a Large Rapidity Gap

2.4.1 Observation of Events with a Large Rapidity Gap at high Q^2

The dominant mechanism of DIS is the hard scattering of the exchanged current from a coloured quark. The colour field between the struck quark and the target remnant is responsible for populating the rapidity interval between them with final state hadrons. The energy flow distributions in fig. 2.4 show that this paradigm is applicable for the bulk of the DIS events.

However, a class of events has been observed in which there are no hadrons close to the proton beam direction. Expressed in terms of the pseudorapidity η, these events exhibit a large difference between the pseudorapidity of the smallest angle measurable in the detector ($\vartheta = 1.5°, \eta = 4.3$) and the pseudorapidity of the cluster in the calorimeter (with an energy deposit in excess of 400 MeV) closest to the proton direction (η_{max}). Figure 2.5 shows the distribution of η_{max} for all DIS events selected according to the criteria outlined in sect. 1.3 and 2.1.

The shaded area represents the expected rate of a Monte Carlo calculation based on a model, which describes the main fraction of DIS events reasonably well. The Monte Carlo events have been passed through the detector simulation and the reconstruction program to be compared directly with the

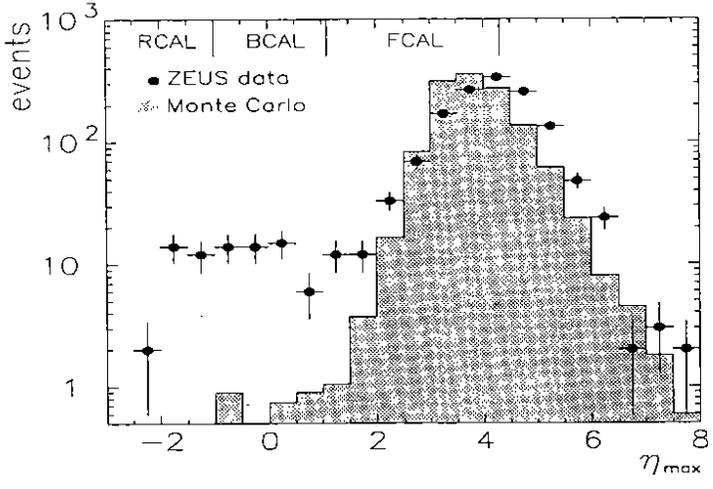

Fig. 2.5. Distribution of η_{max}, the maximum rapidity of a calorimeter cluster with an energy > 400 MeV in an event for data and Monte Carlo events. The boundaries of the calorimeter are indicated. Values of $\eta_{max} > 4.3$ may occur when particles are distributed in several contiguous cells around the beampipe hole in FCAL and combined to one cluster. The number of Monte Carlo events with $\eta_{max} > 1.5$ is normalized to the number of data events in the same η_{max} range.

measured event distribution. There is a significant excess of events over Monte Carlo at small $\eta_{max} < 1.5$. These events are denoted as "large rapidity gap events".

The rate of DIS events in this range as expected from standard DIS models is 4 ± 1. The probability of producing an event with a rapidity gap of more than two units by effects of perturbative QCD has been estimated from $q\bar{q}$ production at LEP to be $< 10^{-3}$ [29]. The background from electron-gas interaction was computed to be 7 ± 3 by Monte Carlo simulation and checked by data from electron pilot bunches. A net excess of 78 ± 10 events remains corresponding to 5.4 % of the total DIS sample.

It should be stressed, that these events are observed in deep inelastic scattering with Q^2 values as high as 100 GeV^2/c^2.

2.4.2 Discussion

The characteristics of the large rapidity gap events were further investigated. Besides the invariant mass W_{DA} of the total hadronic final system as computed from the leptonic variables (eq. 2.5) one has to introduce M_X, the invariant mass of the hadronic system observed in the detector (see fig. 2.6). M_X is determined using the calorimeter cell information, applying an approach similar to the double angle method: $M_X = \sqrt{E_H^2 - p_H^2}$, where E_H and p_H are given by the relationships: $E_H - p_H \cos(\vartheta_H) = 2E_e y_{JB}$, $p_H^2 \sin^2(\vartheta_H) = Q_{DA}^2(1 - y_{JB})$ and $cos(\vartheta_H) = \sum_h p_z / |\sum_h p|$. The sum in the last expression runs over all calorimeter cells which are not assigned to the electron. The qualitative different event topologies of large rapidity gap events and standard DIS events are sketched in fig. 2.6.

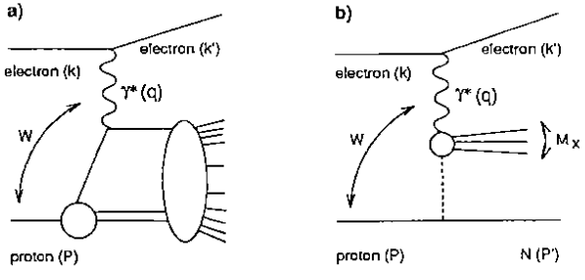

Fig. 2.6. Schematic diagram of particle production in deep inelastic e-p scattering (a) and diffractive dissociation in e-p interaction (b). N represents a proton or low mass nuclear system.

Figure 2.7 compares the correlation between W and M_X for the large rapidity gap events and the DIS data sample. The large rapidity gap events populate the whole W range, but show small values of M_X, independent of W, whereas for the standard DIS events a clear positive correlation between W and M_X is seen.

The fraction of large rapidity gap events in the DIS sample is shown as shown as function of W (fig. 2.8a). In the upper part of the W intervall the dependence of this fraction is compatible with constancy. At low values of W the efficiency of selecting this type of events by selection criteria decreases, because the distributions of DIS events and large rapidity gap events overlap and do not allow a clean separation of these two event classes (compare fig. 2.7). This makes it plausible, why this class of events could not be identified in previous DIS experiments.

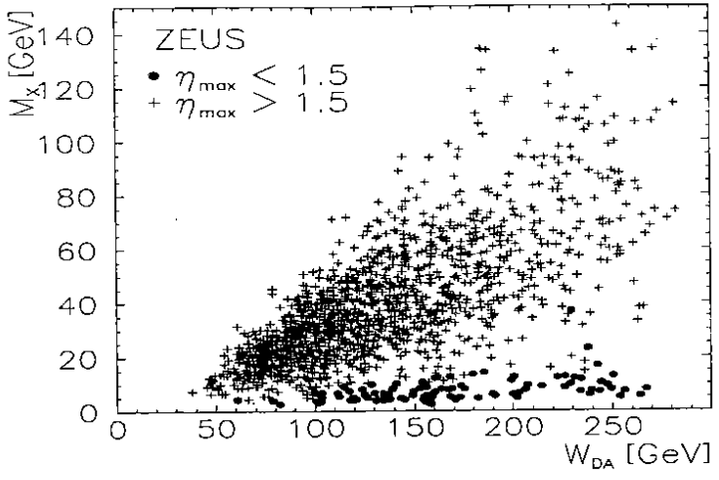

Fig. 2.7. Correlation between the invariant mass M_X of the hadrons observed and the invariant mass W_{DA} of the $\gamma^* p$ system.

The event rate as a function of M_X^2 is presented in fig. 2.8b. Above M_X^2 of $25\,\mathrm{GeV}^2$ the distribution is steeply falling with M_X^2. The data are not corrected for trigger efficieny and detector acceptance.

The absence of a strong W-dependence of the relative fraction of these events in the DIS sample for $W > 150\,\mathrm{GeV}$ and the steeply falling shape of the M_X^2-distribution are suggestive for a diffractive like interaction between the highly virtual photon and the proton.

These results are of particular interest, as they link the field of Regge theory, which describes successfully the behaviour of total, elastic and diffractive like cross sections [30, 31], and perturbative QCD applied in hard parton scattering processes.

Regge-type models for diffractive reactions involve the exchange of a pomeron, the nature of which is still poorly understood [33]. Recently data from the UA8 experiment gave evidence for jets with high transverse momentum in diffractive like $p\bar{p}$ collisions [34], which could be interpreted as hard scattering from partons of a pomeron.

The large rapidity gap events seen at HERA can be understood as the result of a γ^*-pomeron interaction. The absence of any hadrons close to the proton is consistent with the hypothesis of the exchange of a colourless object between the proton and the virtual photon.

More experimental information is needed to answer several open questions:

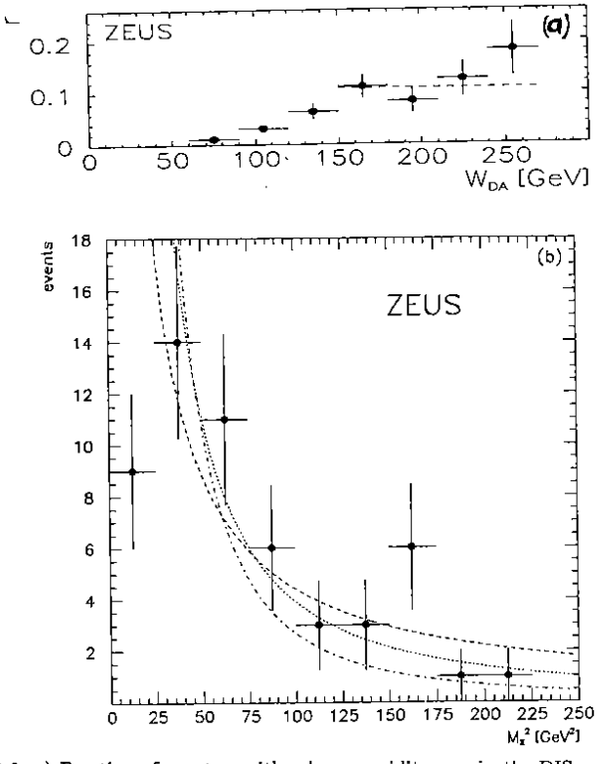

Fig. 2.8. a) Fraction of events r with a large rapidity gap in the DIS event sample. b) Distribution of M_X^2 for events with a large rapidity gap, $\eta_{max} < 1.5$ and $W_{DA} > 150\,\mathrm{GeV}$. The lines show a $1/M_X^2$, $1/M_X^3$, $1/M_X^4$ dependence (full, dashed and dashed dotted line resp.) The data are not corrected for acceptance ans smearing.

besides the proof of the existence of a diffractive cluster, I consider the study of the hardness of the γ^*-pomeron interaction as an important issue. This can be most directly tested by measuring the p_t with respect to the virtual photon of the hadron closest to the rapidity gap in a system where the proton and virtual photon momenta are collinear.

3 Photoproduction at HERA

The non trivial structure of the photon is manifest in the complicated decomposition of the total photoproduction cross section which can be written as:

$$\sigma_{tot}^{\gamma p} = \sigma_{elast}^{\gamma p} + \sigma_{diffr}^{\gamma p} + \sigma_{non-diffr}^{\gamma p} \tag{3.1}$$

where the non diffractive cross section can be splitted in:

$$\sigma_{non-diffr}^{\gamma p} = \sigma_{non-diffr,VMD}^{\gamma p} + \sigma_{resolv}^{\gamma p} + \sigma_{direct}^{\gamma p} \tag{3.2}$$

At low p_t the photoproduction cross section can be described by the vector meson dominance (VMD) model. The elastic, diffractive and non-diffractive part of the VMD-type cross section is denoted by $\sigma_{elast}^{\gamma p}$, $\sigma_{diffr}^{\gamma p}$ and $\sigma_{non-diffr,VMD}^{\gamma p}$, respectively. At HERA the invariant mass of the γp reaction is larger than in previous experiments by almost a factor of ten. Hence the region of high p_t can be explored, where the resolved and the direct component of the non diffractive cross section ($\sigma_{resolv}^{\gamma p}$, $\sigma_{direct}^{\gamma p}$) are expected to be dominant. The three non-diffractive processes are schematically sketched in fig. 3.1.

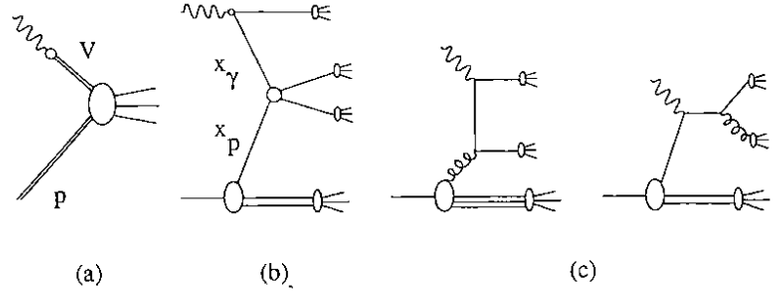

Fig. 3.1. Schematic diagrams of the non-diffractive contributions to the total photoproduction cross section: a) non diffractive part described by the VMD model, b) resolved and c) direct photoproduction.

3.1 Total Cross-Section and General Characteristics of Photoproduction

In most of the e-p reactions at HERA a quasi-real photon is exchanged. The cross section for e-p scattering at very low Q^2 can be written in terms of σ_T and σ_L, the cross sections for transversely and longitudinally polarized photons

respectively:

$$\frac{d^2\sigma_{ep}}{dydQ^2} = \frac{\alpha}{2\pi}\frac{1}{Q^2}\left[\frac{1+(1-y^2)}{y}\sigma_T(y,Q^2) + 2(1-y)\sigma_L(y,Q^2)\right] \qquad (3.3)$$

where y is defined in eq. 2.6. Here σ_L can be neglected and $\sigma_T(y,Q^2) \approx \sigma_T(y)$, because of the small Q^2-values ($< 10^{-2}\,\mathrm{GeV}^2/\mathrm{c}^2$). Integrating over the y- and Q^2-interval defined by the experimental acceptance, one can express $\sigma_{tot}^{\gamma p}$ in terms of the measured e-p cross section.

A first measurement of the total photoproduction cross section, based on the data from the first short data-taking period has been presented [35]. Details of the event selection and the corrections can be found in [2]. The result from the analysis of all data from the year 1992 is shown in fig. 3.2 together with the result of the H1 experiment [36] and the large number of data points from fixed target experiments at low W. The statistical and systematic errors are given in table 3.1.

γp process	fraction of the total cross section		
	measured value	$\pm$ stat. error	$\pm$ syst. error
non-diffractive	0.65	$\pm$0.02	$\pm$0.06
diffractive	0.24	$\pm$0.01	$\pm$0.05
elastic	0.11	$\pm$0.01	$\pm$0.04

Tab. 3.1. Table of partial cross sections for photoproduction at $< W >= 181 GeV$. The value for the total cross section $\sigma_{tot}^{\gamma p}$ as measured by ZEUS is: 133 ± 2.5 (stat.) ± 16 (syst.) μb

The value of $\sigma_{tot}^{\gamma p}$ at high W is compatible with energy independence or rather small increase with W. The experimental result is compared with various predictions of $\sigma_{tot}^{\gamma p}$ at high energies. The solid lines represent Regge-type analyses, which have used the low energy data and existing parametrizations of the proton structure functions [32, 37]. The third predictions is based on the assumption that the total cross section is the sum of a soft and a hard component [38]. The contribution of the latter depends critically on the photon structure function and the cut-off in the transverse momentum p_t^{min}, which is the lower limit of the integration for the hard scattering process. For the prediction shown in fig. 3.2 the parametrization for F_2^γ of Dress and Grassie ([39]) and a value for p_t^{min} of 2 GeV/c was used. The use of other parametrizations of F_2^γ ([40]) or lower values of p_t^{min} lead to a much steeper rise of $\sigma_{tot}^{\gamma p}$ with W.

The experimental results favour the prediction by the Regge-type analysis.

Also the global event characteristics, i.e. the energy deposit in the different parts of the calorimeter (FCAL, BCAL, RCAL) can be well described by models which assume a hadron like interaction of the photon. The partial cross sections for elastic, diffractive and non-diffractive reactions can be obtained by describing the distributions of the global event variables with Monte

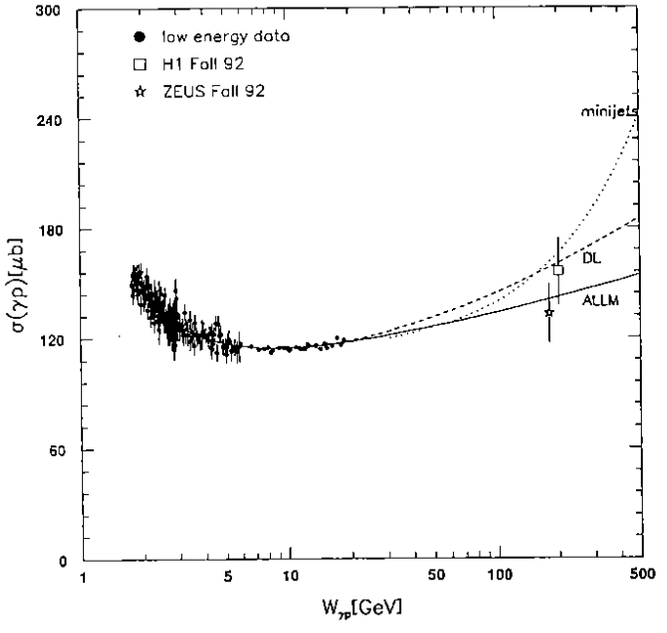

Fig. 3.2. Total photoproduction cross section measured by ZEUS (updated result based on all data from 1992), compared with the result of H1 [36] and low energy data. The curves show prediction by Regge-type models (DL [32] and ALLM [37]), and one of the calculations which involve soft and hard γp-processes with $p_t^{min} = 2.0$ GeV/c and F_2^γ from [39]

Carlo data, which include all those processes, and leaving the relative fraction of the contributions as free parameters. The result is given in table 3.1.

3.2 Hard Scattering in Photoproduction

3.2.1 Observation of Hard Scattering in Photoproduction

Evidence for hard photon scattering has been found in two-photon reactions in e^+-e^- collisions [41] as well as in fixed target experiments [42, 43]. But the restricted phase space available in these experiments has not allowed the observation of two-jet production.

At HERA, for the first time, di-jet events were unambiguously observed. In fig. 3.3 the transverse energy with respect to the beam direction in the η-

φ-plane measured in the calorimeter ($E_\perp$), is shown for two events, where η is the pseudorapidity ranging from +4.3 (FCAL beampipe cut) to -3.8 (RCAL beampipe cut) and φ is azimuthal angle around the beam axis.

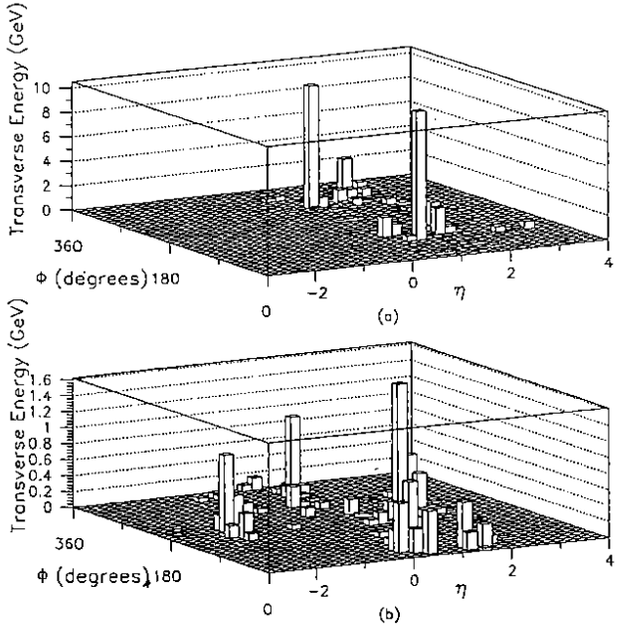

Fig. 3.3. Transverse energy distribution in the η-φ plane of candiates for photoproduction events with two jets: a) direct photoproduction, b) resolved photoproduction

Figure 3.3a shows a candidate for a direct photon event with two distinct jets in the central part of the calorimeter, balanced in φ. In direct photon events the photon couples directly to a parton pair (see fig.3.1c).

In fig. 3.3b another di-jet event is shown, where in addition to the two jets some energy is deposited in the RCAL. This energy deposit arises most likely from the photon remnant (compare fig. 3.1b).

For this analysis, in addition to the basic event selection (sect. 1.3), a minimum amount of energy deposit in the calorimeter was required. Cuts on y_{JB} ($0.2 < y_{JB} < 0.7$) and $y_e = 1 - \frac{E'_e}{2E_e}(1+\cos\vartheta_e) < 0.7$ are imposed to reject background events from p-gas interactions and DIS.

In this event sample jets were searched using cone algorithms in the η-φ-space based on the 'Snowmass' convention [44]. The search was restricted to the angular range of $\vartheta > 10°$.

A comparison of measured differential jet multiplicities $\frac{dN_{jet}}{dE_{\perp,jet}}$ for $E_{\perp,jet} >$ 5 GeV and model calculations shows that the high p_t photoproduction events are in good agreement with the expectation of the hard QCD processes, direct and resolved photoproduction. The soft γ-p scattering as described in the VMD modell gives a much steeper falling p_t-distribution.

For the subsample of events with two jets the energy deposited in the RCAL (E_{RCAL}) is plotted versus the minimum pseudorapidity of either of the two jets (fig. 3.4). There is a sizable amount of energy in the RCAL

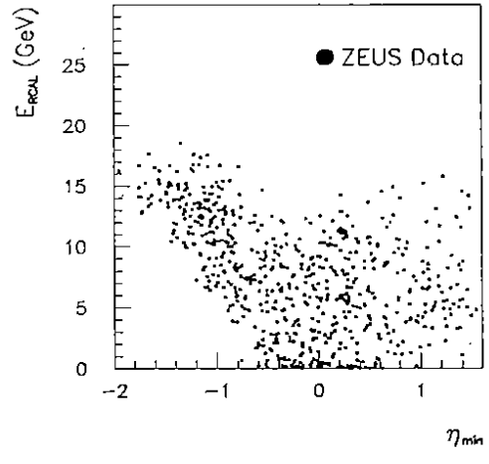

Fig. 3.4. Energy deposited in RCAL as function of the minmum rapidity of either jets in di-jet events; the boundary between RCAL and BCAL is at $\eta_{min} = -1.1$

even for those events, where both jets are in the forward hemisphere, i.e. $\eta_{min} > 0$, and well separated in space from the RCAL. This proves that resolved photoproduction events can be individually selected and studied at HERA.

3.2.2 Separation of Direct and Resolved Photoproduction

Photoproduction events with two jets can be used to distinguish between the resolved and direct processes. The fractional momenta of the partons, which

participate in the hard scattering process, can be inferred from the two final state partons, and hence from the jets observed. Let x_γ (x_p) be the fraction of the four-momentum of the photon (proton) carried by the initial state partons. From conservation of energy and momentum [45]:

$$x_\gamma = \frac{(\sum_{had} E - p_z}{2E_\gamma)_{jets}} \tag{3.4}$$

$$x_\gamma^{meas} = \frac{(\sum_{cells} E - p_z}{2E_e y_{JB})_{jets}} \tag{3.5}$$

where E_γ is the photon energy. The sums in equ. 3.4 and 3.5 run over all particles in the jets respectively over all calorimeter cells assigned to one of the jets. The requirements $|\eta^{jet_1} - \eta^{jet_2}| < 1.5$ and $|\varphi^{jet_1} - \varphi^{jet_2}| > 120°$ are imposed to improve the resolution of x_γ^{meas}. The estimated error of x_γ^{meas} is $14 - 22\,\%$.

The x_γ^{meas} distribution for the 193 di-jet events which passed these cuts, as shown in (fig. 3.5) is falling in the range of 0.2-0.6, but rises significantly towards higher x_γ^{meas}.

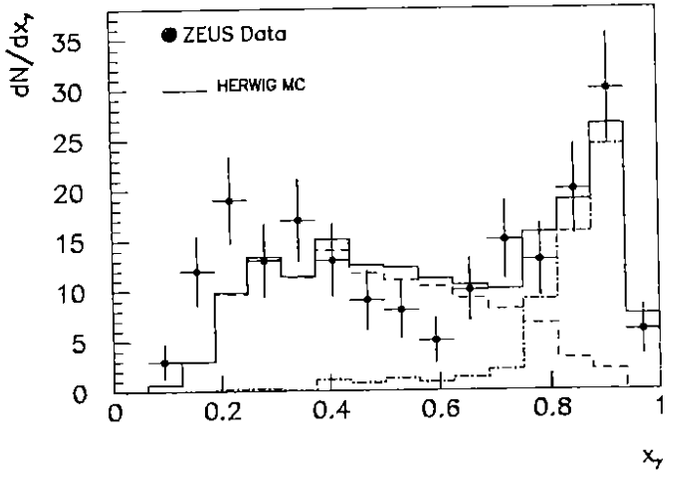

Fig. 3.5. Distribution of x_γ^{meas} for di-jet events in photoproduction. Monte Carlo calculation: dashed and dashed dotted line show the contributions of the resolved and direct γp-processes separately; the full line is the sum of both.

For direct photon events the value of x_γ is equal to unity. Effects of the limited detector resolution and of the jet reconstruction lead to a shift to lower values and a broadening of the peak in the x_γ^{meas} distributions. The full line shows the sum of the independently normalized contributions from resolved and direct processes using the shape predicted by Monte Carlo data which have been passed through a full detector simulation and the reconstruction program. In the central and high region of x_γ^{meas} the measured distribution is well reproduced by the combined fit. The resolved photoproduction component tends to vanish, as x_γ^{meas} approaches unity (dashed line). From this comparison with the Monte Carlo calculation, most of the events in the observed peak at high x_γ^{meas} can be attributed to direct photoproduction events. This result holds also if one uses different parametrizations of the photon and proton structure functions. A possible contamination from diffractive events was studied and found to be negligible.

In conclusion, the x_γ^{meas} distribution shows a clear peak at high x_γ^{meas}, which can be attributed to the presence of direct photoproduction events. Fits to $x\gamma$ distributions will allow a determination of the cross sections for resolved and direct photoproduction.

4 Search for New Particles

Any experiment which enters a higher energy regime, will search for violations of the Standard Model (S.M.) under these new conditions. A conspicuous sign for physics beyond the S.M. is the appearance of new particles. Extensions and models going beyond the S.M. make a number of predictions in this respect.

Although the integrated luminosity in 1992 was small as compared to the design luminosity in 1993, in certain cases new constraints on non standard physics models could be placed.

4.1 Search for Leptoquarks

Leptoquarks, which could be created by new forces between quarks and leptons, are predicted in many extensions of the S.M. [46, 47]. At HERA leptoquarks are produced most favourably as resonances in the s-channel (fig. 4.1). These events would not have the steeply falling Q^2-dependence, but would populate a narrow x-band in the $x - Q^2$-plane and show up as a peak in the x-distributions at $x = M_{LQ}^2/s$.

No such accumulations have been seen in the data [48]. The cross section depends on the coupling $g = \sqrt{g_L^2 + g_R^2}$ between the leptons and quarks, the strength of which is unknown; g_L and g_R are the left handed and right handed coupling constants, respectively. Assuming $g_L = 0.31$ or $g_R = 0.31$, which corresponds to the electromagnetic coupling strength, one can infer lower limits for the mass of various species of leptoquarks. A compilation of these limits at the 95% confidence level is given in table 4.1.

scalar leptoquark species	mass limit (GeV) L.H.	R.H.	vector leptoquark species	mass limit (GeV) L.H.	R.H.
S_0	176	183	$V_{\frac{1}{2}}$	173	207
$\tilde{S}_0$	—	151	$\tilde{V}_{\frac{1}{2}}$	202	—
$S_{\frac{1}{2}}$	93	117	V_0	120	120
$\tilde{S}_{\frac{1}{2}}$	93	—	$\tilde{V}_0$	—	120
S_1	188	—	V_1	137	—

Tab. 4.1. Mass limits (GeV) on scalar and vector leptoquarks for $g_L = 0.31$ or $g_R = 0.31$ at 95% CL.

4.2 Search for Excited Electrons

The existence of three lepton families (e, μ, τ) give rise to the question, whether leptons are composited objects. The search for excited leptons is a direct way to investigate the substructure in the fermion sector. Limits on the compositeness scale have been derived mainly in e^+-e^--experiments [50]. At HERA excited electrons, e^*, with masses m_{e^*} up to the total c.m. energy of $\sqrt{s} = 296$ GeV would be produced in a process $e\,p \rightarrow e^*\,X$. This allows to search for the decay modes $e^* \rightarrow e\gamma$, $e^* \rightarrow e\,Z$ and $e^* \rightarrow \nu\,W$.

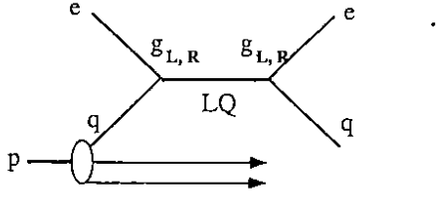

Fig. 4.1. s-channel production of a leptoquark.

The production cross section is a function of the mass m_{e^*}, the compositeness scale Λ and the parameter of the coupling of the γ to the e^*, $c_{\gamma e^* e}$ and $d_{\gamma e^* e}$. For all three decay modes the number of signal events remaining after the selection cuts is consistent with the estimated backgroud rate [49].

Figure 4.2 shows at the 95% CL., the limits on the product of the coupling strength and the branching ratio B as a function of the mass m_{e^*}. The limits were extracted assuming Poisson statistics and including the systematic uncertainties in the production cross section, tagging efficiencies and integrated

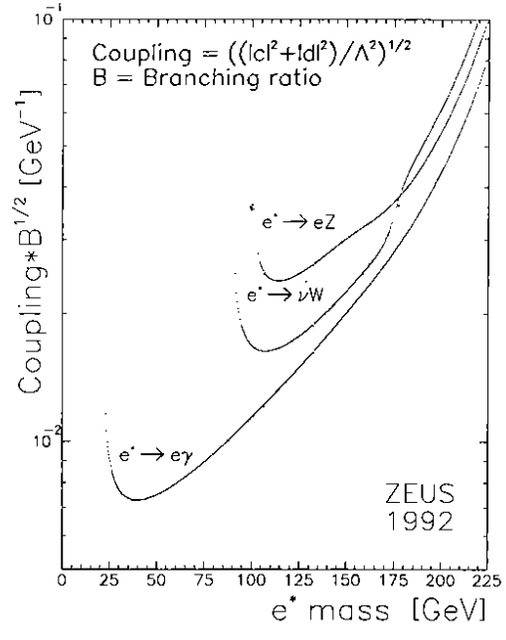

Fig. 4.2. 95% confidence level upper limit on the product of the coupling and square root of the branching ratio for the $e\gamma$, $e\,Z$ and $\nu\,W$ decay mode as function of the e^* mass.

luminosity. In contrast to e^+-e^--experiments, at HERA upper limits for inclusive production of excited electrons can be set above the Z-mass.

5 Concluding Remarks

Results from the ZEUS experiment, which are based on the analysis of the data from the data-taking periods in 1992, have been reported. In all three subfields – deep inelastic scattering, photoproduction and new particle search – many new and interesting results have been obtained, which should initiate new theoretical work.

The new data for the structure function F_2 at x-values two orders of magnitude lower than before are an important input for the understanding of the parton densities at low x. The discovery of a class of diffractive events at high

Q^2 is under active discussion. The measurement of the total photoproduction cross section at very high c.m. energies indicates a energy dependence similar to that for $p\bar{p}$-scattering. This result is valuable for planning future high energy physics experiments.

In view of the much larger amount of data taken in 1993, a significant increase of the accuracy and refinement of the analysis can be expected.

Acknowlegdements

It is a pleasure for me to thank Suzana Dubickova, Stanislav Dubnicka and their colleagues for organizing this conference in such a nice and excellent manner. I am grateful to the members of the ZEUS Collaboration for many helpful discussions and comments.

References

[1] ZEUS Collaboration, 'The ZEUS Detector', Status Report 1993.

[2] ZEUS Collaboration, M. Derrick et al., Phys. Lett. B293 (1992) 465.

[3] M. Derrick et al., Nucl. Instr. Meth. A309 (1991) 77.
A. Andresen et al., Nucl. Instr. Meth. A309 (1991) 101.

[4] A. Bernstein et al., to be subm. to Nucl. Instr. Meth..
I. Gialas, Proc. of Second Int. Conf. on Calorimetry for High Energy Physics, Capri (1991) 162.

[5] C.B. Brooks et al., Nucl. Instr. Meth. A283 (1989) 477.

[6] N. Harnew et al., Nucl. Instr. Meth. A279 (1989) 290,
B. Foster et al., Proc. 3rd Int. Conf. on Advanced Technology and Particl Physics, Como (1992) and Oxford Univ. prepr. OUNP-92-14 (to be publ. in Nucl. Instr. Meth.).

[7] J. Andruszkow et al., DESY 92-066 (1992)

[8] Recent data from charged lepton scattering experiments:
NMC Collaboration, P. Amaudruz et al., Phys. Lett. B295 (1992) 159.
BCDMS Collaboration, A.C. Benvenuti et al., Phys. Lett. B237 (1990) 592.
L.W. Whitlow et al., Phys. Lett. B250 (1990) 193 (reanalysis of SLAC/MIT data).

[9] Recent data from neutral lepton scattering experiments:
CCFR Collaboration, W.C. Leung et al., Nevis prepr. #1460 (1992) (subm. to Phys. Lett.),
CCFR Collaboration, P.Z. Quintas et al., Phys. Rev. Lett. 71 (1993) 1307.
CDHSW Collaboration, P. Berge et al., Z. Phys. C49 (1991) 187.

[10] N. Schmitz, Int. J. Mod. Phys A8 (1993) 2026.

[11] T. Sloan, G. Smadja, R. Voss, Phys. Rep. 162 (1988) 45.

[12] S. Bentvelsen, J. Engelen, P. Kooijman, Proc. of Workshop on 'Physics at HERA', DESY (1992), p 23.

[13] F. Jacquet, A. Blondel, Proc. of Workshop on study of an ep facility for Europe, DESY 79/48 (1979) 391.

[14] A. Kwiatkowski, H. Spiessberger, H.-J. Möhring, Proc. of Workshop on 'Physics at HERA', DESY (1992), p 1294.
A. Kwiatkowski, H. Spiessberger, H.-J. Möhring, Z. Phys. C50 (1991) 165.

[15] S. Bentvelsen, PhD thesis (Univ. of Amsterdam) 1993
(in preparation),
F. Chlebana, PhD thesis (Univ. of Toronto) 1993
(in preparation).

[16] ZEUS Collaboration, M. Derrick et al., DESY 93-110 (August 1993) (accepted by Phys. Lett.).

[17] E. Levin, Proc. of the Workshop 'QCD - 20 years later', Aachen (1992) p 310.

[18] CTEQ Collaboration, J. Botts et al., Phys. Lett. B304 (1993) 391.

[19] A.D. Martin, R.G. Roberts, W.J. Stirling, Phys. Lett. B306 (1993) 145.

[20] M. Glück, R. Reya, A. Vogt, Phys. Lett. B306 (1993) 145.

[21] ZEUS Collaboration, M. Derrick et al., Phys. Lett. B306 (1993) 158.

[22] I. Park, contrib. to the Int. Europhysics Conf. on High Energy Physics, Marseille July 1993.

[23] ZEUS Collaboration, M. Derrick et al., Z. Phys. C59 (1993) 231.

[24] EMC Collaboration, J. Ashman et al., Z. Phys. C52 (1991) 361.

[25] N. Magnussen et al., Proc. of Workshop on 'Physics at HERA', DESY (1992), p 1167.

[26] O. Deppe, T. Haas, N. Pavel, Zeus int. rep. 93-106 (1993) and
O. Deppe, Diploma thesis (Univ. of Hamburg) in preparation.

[27] G. Ingelmann, Proc. of Workshop on 'Physics at HERA', DESY (1992), p 1366.

[28] B. Anderson et al., Phys. Rep. 97 (1983) 31.

[29] J.D. Bjorken, S.J. Brodsky, H.J. Lu, Phys. Lett. B286 (1992) 867.

[30] R.D. Field, G.C. Fox, Nucl. Phys. B80 (1974) 367.

[31] A. Donnachie, P.V. Landshoff, Nucl. Phys. B231 (1984) 189 and Nucl. Phys. B297 (1992) 690.

[32] A. Donnachie and P.N. Landshoff) Nucl. Phys. B244 (1984) 322.
P.N. Landshoff, Nucl. Phys. B (Proc. Suppl.) 18C (1990) 211.

[33] K. Goulianos, Nucl. Phys. B, (Proc. Suppl.) 12 (1990) 110.

[34] UA8 Collaboration, R. Bonino et al., Phys. Lett. B211 239.
and A. Brandt at el., Phys. Lett. B297 (1992) 417.

[35] B. Löhr, Proc. of the Int. Conf. on High Energy Physics, Dallas, August 1993, p 2037.

[36] H1 Collaboration, T. Ahmed et al., Phys. Lett. B299 (1993) 469.

[37] H. Abramowicz, E.M. Levin, A. Levy, U. Maor, Phys. Lett. B269 (1991) 465.

[38] R.S. Fletcher et al., Phys. Rev. D45 (1992) 377.
J.R. Forshow, J.K. Storrow, Phys Lett. B268 (1991) 116.

[39] M. Drees, K. Grassie, Z. Phys. C28 (1985) 451.

[40] H. Abramowicz, K. Charchula, A. Levy, Phys. Lett. B269 (1991) 458.

[41] AMY Collaboration, R. Tanaka et al., Phys. Lett. B277 (1992) 215.

[42] NA14 Collaboration, E. Auge et al., Phys. Lett. B168 (1986) 163,
and Phys. Lett. B182 (1986) 409.

[43] WA69 Collaboration, R.J. Apsimon et al., Z. Phys. C43 (1989) 63 and C46 (1990) 35.

[44] J. Huth et al., Proc. of the 1990 DPF Summer Study on High Energy Physics,
Snowmass, Colorado (ed. World Scientific 1992) p 134.

[45] J.F. Owens, Phys. Rev. D21 (1979) 54.

[46] J.C. Pati, A. Salam, Phys. Rev. Lett. 31 (1975) 661 and Phys. Rev. D10 (1974) 275.

[47] W. Buchmüller et al. Phys. Rep. B191 (1987) 442.
B. Schrempp, Proc. of Workshop on 'Physics at HERA', DESY (1992), p 1034.

[48] ZEUS Collaboration, M. Derrick et al., Phys. Lett. B306 (1993) 173.

[49] ZEUS Collaboration, M. Derrick et al., DESY 93-075 (accepted by Phys. Lett.)

[50] ALEPH Collaboration, D. Buskulic, et al., Z. Phys. C59 (1993) 215.